

Simultaneously Enhancing Direct-Current Density and Lifetime of Tribovoltaic Nanogenerator via Interface Lubrication

Wenyan Qiao, Zhihao Zhao, Linglin Zhou, Di Liu, Shaoxin Li, Peiyuan Yang, Xinyuan Li, Jiaqi Liu, Jie Wang,* and Zhong Lin Wang*

Tribovoltaic nanogenerators (TVNGs) present great properties such as high direct-current density and continuous output performance, which has great potential to solve the power supply problem for miniaturized electronic devices. However, the severe wear problem of TVNG causes rapid attenuation of current density, which is difficult to realize long-term operation with high output. In this work, an effective strategy via interface lubrication is proposed to enhance the direct-current density and lifetime of TVNGs simultaneously. The water-based graphene oxide solution is utilized as a lubricant, which can increase the sliding surface carriers to enhance current density, and reduce the wear between the copper and the silicon wafer surface due to its excellent lubrication performance. Hence, the TVNG can generate peak current density output $\approx 775 \text{ mA m}^{-2}$, accompanied with 31 mC m^{-2} transfer charges density. The TVNG via interface lubrication can maintain high current output after 30 000 cycles. In addition, it can combine with triboelectric nanogenerator to constitute a dual-type signal sensor, which can be used to monitor bridge vibration and goods' weight. This work provides an effective method to solve the wear problem of TVNG and improve direct-current density simultaneously, which will accelerate the practical application of TVNGs in the future.

sensors are emerging, which are applied in sensor networks, personal health monitoring, artificial intelligence, big data, and the internet of things (IoT).^[1–8] Currently, many sensors and devices are powered by batteries and external chargers, which require more maintenance and replacement costs.^[9] Hence, some features, e.g., self-powered, high output, long-life, and continuous output performance, are needed to power distributed sensors and electronic devices in the micro and renewable power supply systems.

Tribovoltaic nanogenerator (TVNG) can generate direct-current (DC) due to the tribovoltaic effect, which has great features of low matching resistance, high current density, and continuous output performance, showing its great potential to solve the power supply problem for distributed electronic devices.^[10–27] However, the solid–solid hard contact of TVNG will cause the interlocking between atoms on the contact interface, resulting in the increase of friction stress and aggravation of wear problem.^[28] The severe wear problem will cause rapid attenuation of output performance, thus, it is difficult for TVNG to realize long-term operation with high current density. Meanwhile, the wear problem will also increase the device replacement costs and affect the sensitivity of TVNG-based self-powered system. To reduce the wear problem of TVNG, various methods were proposed to improve its lifetime, such as optimizing friction pairs or adding lubricating oil. Recently, tribovoltaic devices based on W/WO₃ Schottky junction was proposed to improve the lifetime of TVNG with the value of >1000 cycles.^[29] TVNG based on MXene-silicon heterojunctions was proposed, which can reach a high output peak current of 22 μA , as well as the enhanced lifetime of over 1800 cycles.^[30] In addition, macro-superlubric TVNG can operate stably for nearly 10 000 cycles.^[31] By adding organic lubricating oil, the TVNG can increase its lifetime to 20 000 cycles, but the addition of lubricating oil cannot achieve high output and even slightly decrease the output.^[32] It can be seen that high current output and long-term lifetime of TVNG are not compatible in current research, which is not conducive for the practical application of TVNG. Hence, an effective strategy is highly desired to simultaneously enhance the current output performance and improve the lifetime of TVNG.

1. Introduction


With the development of micro and renewable energy, a large number of miniaturized electronic devices and distributed

W. Qiao, Z. Zhao, L. Zhou, D. Liu, S. Li, P. Yang, X. Li, J. Liu, J. Wang, Z. L. Wang

Beijing Institute of Nanoenergy and Nanosystems
Chinese Academy of Sciences
Beijing 100083, P. R. China
E-mail: wangjie@binn.cas.cn

W. Qiao, Z. Zhao, L. Zhou, D. Liu, S. Li, X. Li, J. Wang, Z. L. Wang
School of Nanoscience and Technology
University of Chinese Academy of Sciences
Beijing 100049, P. R. China

Z. L. Wang
School of Materials Science and Engineering
Georgia Institute of Technology
Atlanta, GA 30332, USA
E-mail: zhong.wang@mse.gatech.edu

 The ORCID identification number(s) for the author(s) of this article can be found under <https://doi.org/10.1002/adfm.202208544>.

DOI: 10.1002/adfm.202208544

Here, an interface lubrication strategy is proposed to improve the direct-current output and lifetime of TVNG at the same time. The water-based graphene oxide (GO) solution is utilized as lubricant at the sliding interface, which has good electric performance to increase the sliding surface carriers, and has a lubricating property to reduce the wear between the copper-based monolayer graphene (Cu-G) film and the silicon wafer surface. The TVNG via interface lubrication can generate ultra-high peak current output of 155 μA (corresponded current density of 775 mA m^{-2}), accompanied with transfer charges of 6.2 μC (corresponded charge density of 31 mC m^{-2}). The TVNG via interface lubrication can remain $\approx 92\text{--}95\%$ electric output after 30 000 operation cycles. In addition, based on the high output of TVNG, its DC signal can combine with conventional alternating-current triboelectric nanogenerator (AC-TENG) to constitute a self-powered dual-type signals (DS) sensor, which can generate AC signal in the safe zone, and once in outside the safe zone, will produce DC signal and generate signal light alarm. Thus, the DS sensor has great application potential in monitoring bridge vibration and goods' weight monitoring of intelligent factory production line. This work provides an effective strategy to improve the direct-current density and lifetime of TVNG simultaneously and accelerates the future application of TVNG in sensor networks, intelligent factory, and the IoT.

2. Results and Discussion

2.1. Structural and Electric Output Characteristics of the TVNG

The schematic diagram of interfacial lubrication TVNG is shown in Figure 1a, including copper-based monolayer graphene film attached to an acrylic substrate to move on silicon wafer, water-based GO solution as a lubricant between the Cu-G film and the silicon wafer surface. This TVNG is abbreviated as GWS-TVNG. On the back of the silicon wafer, a layer of gold with a thickness of 2 μm is sputtered by magnetron sputtering as the back electrode. The external circuit is connected with the Cu-G film and the gold back electrode. Figure 1b shows a 3D schematic and external circuit of the GWS-TVNG structure. The Cu-G film's position and velocity as functions of time are recorded in Figure 1c(i,ii), and the corresponding short-circuit current output can be seen in Figure 1c(iii) $\approx 45 \mu\text{A}$. In order to better understand the effect of interface lubricant on TVNG's output, we designed four TVNGs structure respectively: i) TVNG-i, constituted by water-based GO solution and silicon wafer (Figure S1a, Supporting Information), ii) TVNG-ii, constituted by Cu-G film and silicon wafer (Figure 1d(i)), iii) TVNG-iii, constituted by Cu-G film, water and silicon wafer (Figure 1d(ii)), iv) GWS-TVNG, constituted by Cu-G film, water-based GO solution and silicon wafer (Figure 1d(iii)). Figure S1a (Supporting Information) shows the structure of TVNG-i, which has a syringe filled with water-based GO solution, and a needle connected with a wire. The needle of the syringe does not directly contact with the silicon wafer (P-type), where the distance between needle and silicon wafer is $\approx 0.5 \text{ mm}$. In addition, the silicon wafer (P-type) is fixed on linear motor, which moves relative to the water-based GO solution to obtain the current output (Figure S1b, Supporting Information) (negative

direction current is $\approx 120 \text{ nA}$). As shown in Figure 1d, compared with the output of the TVNG-i (Figure S1a, Supporting Information) and the TVNG-ii (Figure 1d(i)), the short-circuit current output of the TVNG-iii (Figure 1d(ii)) increases by an order of magnitude to $\approx 18 \mu\text{A}$, indicating that water can effectively improve the output of TVNG. The structure of TVNG-iii is shown in Figure S2a (Supporting Information), its open-circuit voltage is $\approx 80 \text{ mV}$ (Figure S2b, Supporting Information). Furthermore, by replacing the pure water with GO solution, the current output of GWS-TVNG (Figure 1d(iii)) can significantly increase to about two-fold compared with the TVNG-iii (Figure 1d(ii)) due to the better conductivity (Table S1, Supporting Information) of water-based GO solution and graphene's excellent electrical properties which can provide more carriers for sliding friction interfaces. That is, the current output of GWS-TVNG is higher ($\approx 45 \mu\text{A}$) than the previous three TVNGs. Figure 1d demonstrates that both water and graphene are affecting the high-performance output of GWS-TVNG. In addition, by comparing the I - V curves of different kinds of TVNG (Figure S3, Supporting Information), it can be demonstrated that the insulation performance of water is very low and hardly affects the I - V rectification properties.

In order to further clarify the working mechanism of GWS-TVNG, the I - V characteristics of the GWS-TVNG static heterojunction were tested, as shown in Figure 1e. When a forward bias voltage is applied to P-type Si, the output current increases exponentially with the voltage, indicating that the built-in-electric field direction of the heterojunction is from the Cu-G film to P-type Si. In addition, According to the short-circuit current output of the GWS-TVNG during the sliding process in Figure 1f, it can be found that the output current direction is from Cu-G film to P-type Si, which is same as the direction of built-in-electric field.

2.2. Schematic Diagrams of the Working Principle and Electrical Output Performance of the GWS-TVNG (P-type Si)

The GWS-TVNG generates DC signal based on the tribovoltaic effect, when Cu-G film, water-based GO solution, and silicon wafer contact, carrier equilibrium will be re-established at the interface due to different work functions of the materials. During sliding friction, new chemical bonds are formed at the interface, which release energy, called "bindington",^[26,30] and the "bindington" excites electron-hole pairs at the sliding interface. The electron-hole pairs are then separated and expelled out of the Schottky junction under the action of the built-in electric field, resulting in a continuous DC signal.

External circuit state and corresponding band diagram under thermal equilibrium (static) are shown in Figure 2a(i),b. In the state of Figure 2a(i), the Cu-G film and water-based GO solution contact with the silicon wafer (the work function of graphene is $\approx 4.3 \text{ eV}$, copper is $\approx 4.65 \text{ eV}$, and P-type Si is $\approx 4.91 \text{ eV}$ ^[33] (Figure S4, Supporting Information)). The Cu-G film, water-based GO solution, and P-type Si remain relatively stationary, with no current output due to the release of no additional energy in the stationary state. The work function (W_{CW}) of the Cu-G film and water-based GO is smaller than that of (W_{Si}) P-type Si. According to the Equations (1) and (2) shown as follow:

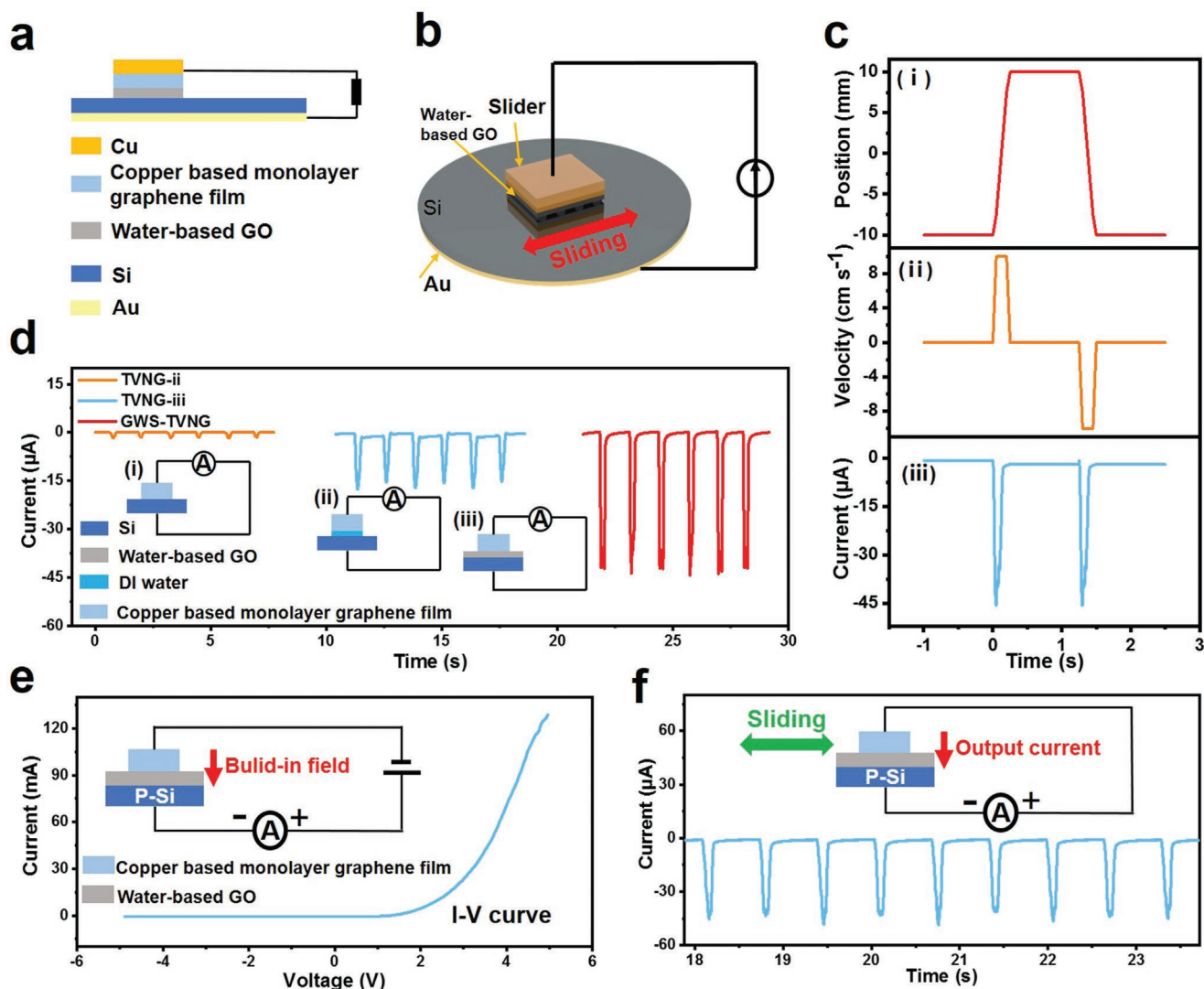


Figure 1. Structural and electric output characteristics of the TVNG. a) The structure and circuit connection of GWS-TVNG. b) A 3D schematic and external circuit of the GWS-TVNG structure. c) The relative position and velocity of the Cu-G film and the silicon wafer as a function of time, and the short-circuit current of GWS-TVNG in the corresponding time. d) Comparing the short-circuit current output of TVNG with three structures. e) *I*-*V* characteristic of the GWS-TVNG. f) Short-circuit current of the GWS-TVNG, the current direction is consistent with the direction of the built-in electric field.

$$E_f = E_0 - W \quad (1)$$

$$E_{f_{Si}} - E_{f_{GW}} = W_{GW} - W_{Si} \quad (2)$$

where E_0 is the vacuum level, it can be known that the fermi level $E_{f_{Si}}$ is smaller than the $E_{f_{GW}}$.

When the Cu-G film is connected to silicon wafer by wires, they form a unified electronic system. Due to the difference in fermi energy levels, when the Cu-G film and the silicon wafer contact under pressure, the equilibrium will be re-established, and the electrons flow to P-type Si, the energy bands bend downward. Form a built-in electric field pointing to P-type Si (Figure 2b). During sliding friction (Figure 2a(ii,iii,iv)), there are two forms of exciting electron-hole pairs. On the one hand, in the process of friction, the bindington excites electron-hole pairs will generate drift motion under the effect of the built-in electric field. On the other hand, some electrons in surface

states will jump to higher energy levels under frictional excitation, overcoming the barrier at the interface. In addition, these holes may also be excited (Figure 2c). Hence, during cyclic sliding friction, DC can be generated in the external circuit.

To further explore the parameters that control the output of the GWS-TVNG (P-type Si), the sliding velocity, the applied pressure, the sliding displacement, the amount of water-based GO solution and the external loads are varied to study their influence on the electrical output (Figure 2d-i). The electrical output can be affected by changing the sliding velocity of Cu-G film (Under conditions of 10 N pressure, 20 mm displacement, and 5 μL water-based GO solution), with the velocity increases, the current output will increase significantly, but the voltage output basically remain unchanged. When the sliding velocity was 0.25 m s⁻¹, the negative current output of GWS-TVNG can reach ≈78 μA (Figure 2d). The output of the GWS-TVNG is enhanced by increasing pressure for a P-type silicon wafer

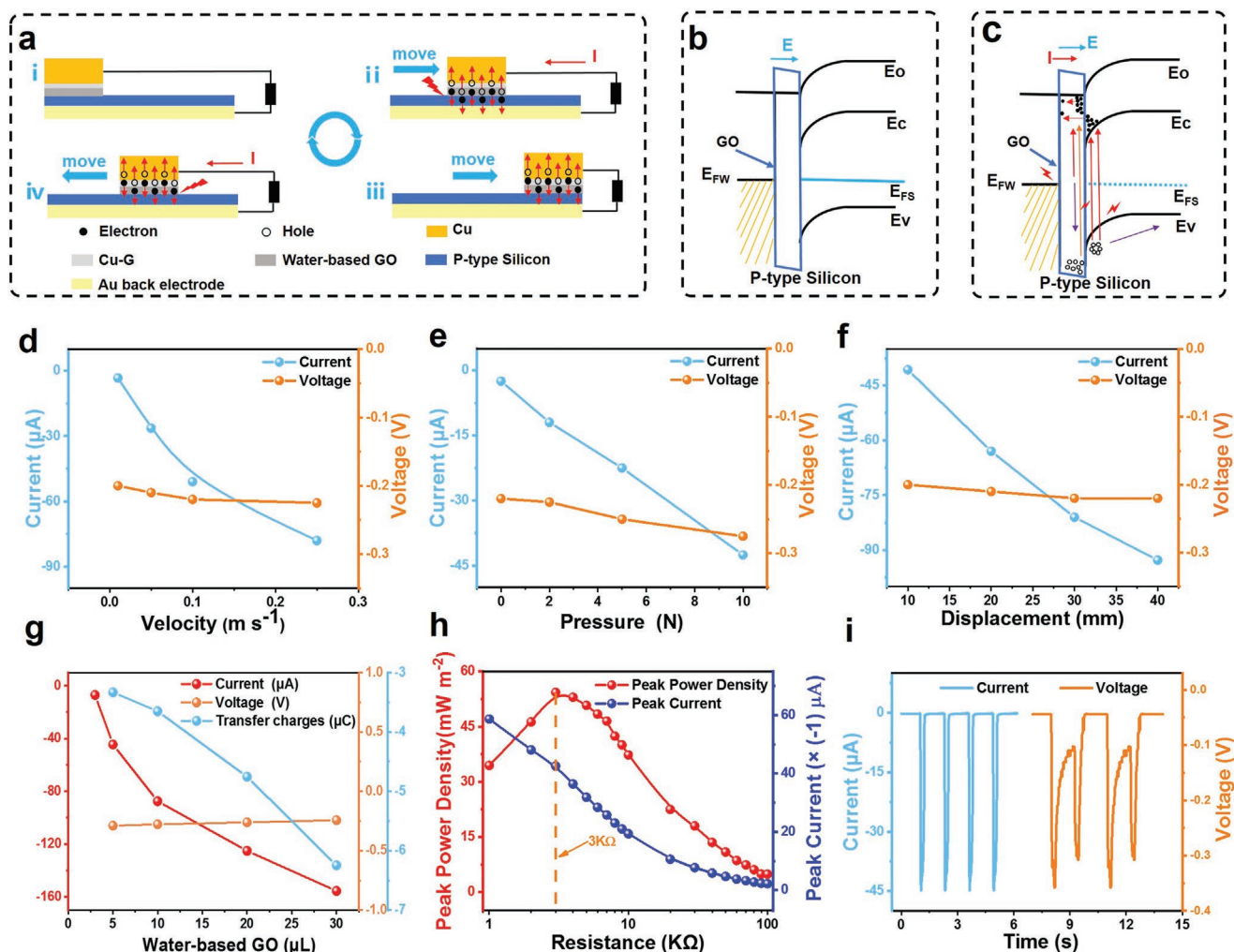


Figure 2. Schematic diagrams of the working principle and electrical output performance of the GWS-TVNG (P-type Si). The Cu-G film moves on P-type Si, and a layer of water-based GO solution is added to the interface. a) Charge transfer schematic diagram. b) The band diagram corresponding to the stationary state in Figure (a). c) The band diagram corresponding to the motion state in Figure (a). The short-circuit current and open-circuit voltage output at different d) velocity, e) pressure, and f) displacement. g) The short-circuit current, open-circuit voltage and transferred charges under different amount of water-based GO solution. h) The peak current and peak power density under different external loads. i) Current and voltage output correspond to the maximum peak power density.

under a sliding velocity of $0.1 m s^{-1}$ (Figure 2e), which is due to possibly more chemical bonds of interface atoms are formed and released, and hence the output increases. The electrical output can be affected by changing the sliding displacement of Cu-G film (Under conditions of 10 N pressure, $0.1 m s^{-1}$ velocity, 8 μL water-based GO solution), with the sliding displacement increases from 10 to 40 mm, the current output will increase negatively from 40.7 to 92.7 μA , but the voltage output basically remains unchanged. In addition, when increases the amount of water-based GO solution from 5 to 30 μL (Figure 2g), the current output and transferred charges can also be enhanced (Under conditions of 10 N pressure, $0.1 m s^{-1}$ velocity, 20 mm displacement), but the voltage output decreased slightly. The TVNG can generate peak current output $\approx 155 \mu A$ (corresponded current density of $775 mA m^{-2}$) and transferred charges output $\approx 6.2 \mu C$ (corresponded charge density of $31 mC m^{-2}$) when the water-based GO solution is 30 μL . In addition, the output

performance of GWS-TVNG can be optimized by changing the concentration of water-based GO solution, Figure S5 (Supporting Information) shows the output performance of GWS-TVNG at different GO concentrations (Motion displacement 20 mm, velocity $0.1 m s^{-1}$, acceleration $2 m s^{-2}$). It can be seen from Figure S5 (Supporting Information) that the output current and voltage tend to increase in the negative direction first and then decrease in the negative direction, and there is an optimal output $\approx 5 mg mL^{-1}$ (Note S1, Supporting Information). After the concentration exceeds $5 mg mL^{-1}$, the output decreases with increasing the concentration. The reason may be that the high concentration of water-based GO solution will form a viscous film on the sliding interface, which reduces the effective sliding contact area on the silicon wafer, so the output will decrease. Figure 2h shows the peak power density and peak current of the GWS-TVNG under different external loads (Water-based GO solution 8 μL , motion displacement 20 mm,

speed 0.1 m s^{-1} , acceleration 2 m s^{-2}). It can be determined that the GWS-TVNG (P-type Si) has a low impedance of $3 \text{ k}\Omega$, and its maximum peak power density is 54.3 mW m^{-2} . Figure 2i shows the current ($\approx 44 \text{ }\mu\text{A}$) and voltage ($\approx 0.3 \text{ V}$) output correspond to the maximum peak power density.

2.3. Schematic Diagrams of the Working Principle and Electrical Output Performance of the GWS-TVNG (N-type Si)

In order to explore the output performance and mechanism of GWS-TVNG with N-type Si, the GWS-TVNG was prepared as shown in Figure 3. When the Cu–G film contacts with N-type Si with a layer water-based GO solution on the interface, a redistribution of carrier concentration at the interface occurs, generating a built-in electric field to point to Cu–G film and water-based GO solution due to the difference in work functions

of these materials (the work function of graphene is $\approx 4.3 \text{ eV}$, copper is $\approx 4.65 \text{ eV}$, and N-type Si is $\approx 4.03 \text{ eV}$ ^[33] (Figure S4, Supporting Information)). A schematic of the external circuit and the corresponding band structure under static state are shown in Figure 3a(i),b. Due to no bindington is released at the static state, there is no DC output. When the Cu–G film moves on the N-type Si with a layer water-based GO solution on the interface, a positive DC current is detected (Figure 3a(ii,iii,iv)). Figure 3c shows the band structure corresponding Figure 3a(ii,iii,iv) under dynamic state.

The output current of GWS-TVNG with N-type Si under various sliding velocities, pressure forces, sliding displacements, and amounts of water-based GO solution is shown in Figure 3d–i, respectively. Figure 3d shows the current and voltage outputs with different sliding velocity (Under conditions of 10 N pressure, 20 mm displacement, $5 \text{ }\mu\text{L}$ water-based GO solution). The output increases as the sliding velocity

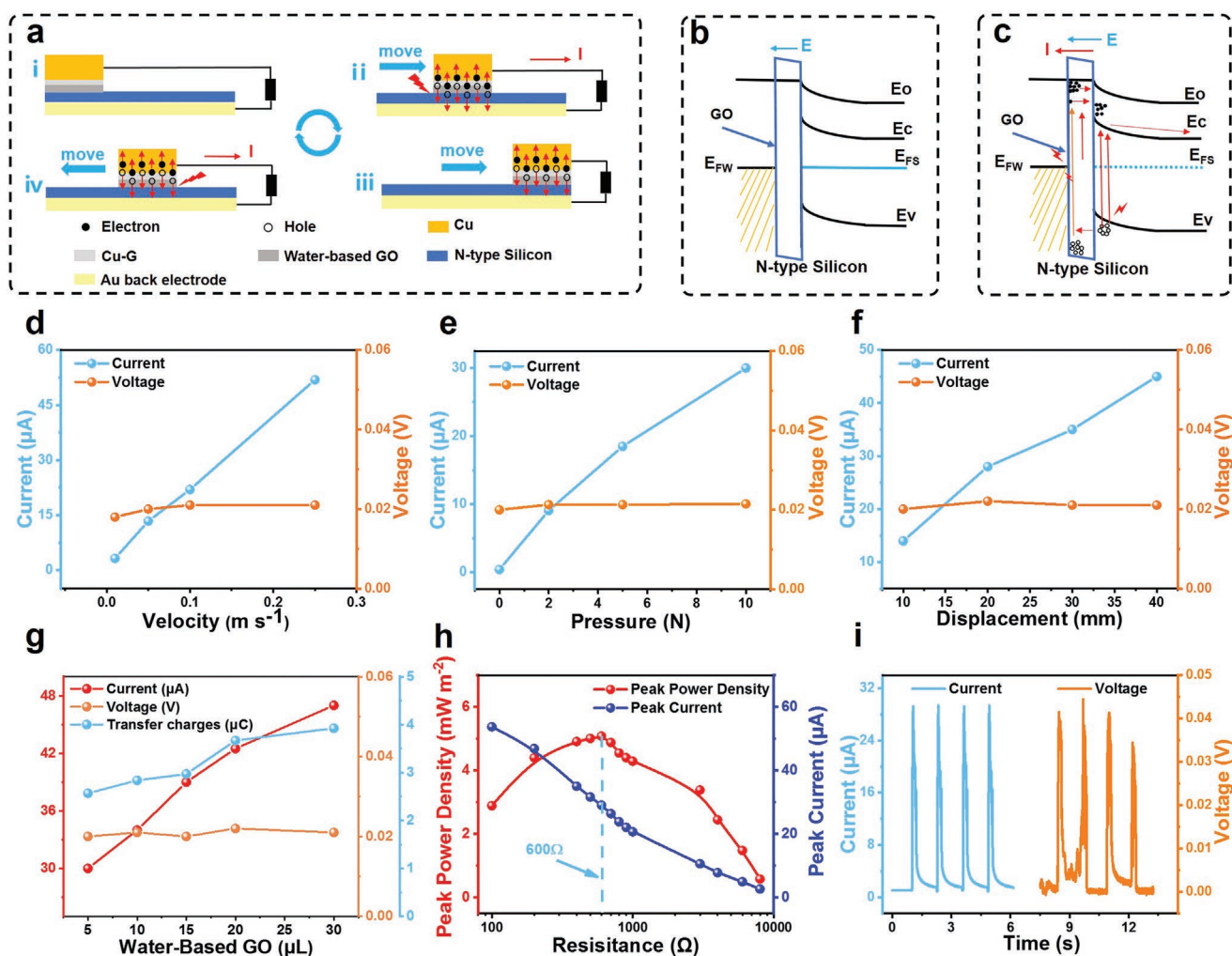


Figure 3. Schematic diagrams of the working principle and electrical output performance of the GWS-TVNG (N-type Si). The Cu–G film moves on N-type Si, and a layer of water-based GO solution is added to the interface. a) Charge transfer schematic diagram. b) The band diagram corresponding to the stationary state in Figure (a). c) The band diagram corresponding to the motion state in Figure (a). The short-circuit current and open-circuit voltage output at different d) velocity, e) pressure, and f) displacement. g) The short-circuit current, open-circuit voltage and transferred charges under different amount of water-based GO solution. h) The peak current and peak power density under different external loads. i) Current and voltage output correspond to the maximum peak power density.

increases, but the voltage output basically remain unchanged. The current of this GWS-TVNG can be enhanced from 9.05 to 30 μA by increasing pressure force from 2 to 10 N (Figure 3e), which is due to possibly more chemical bonds of interface atoms are formed and released, and hence the output increases. With the displacement increase from 10 to 40 mm (Figure 3f), the current output increases from 14 to 45 μA , but the voltage output basically remain unchanged. Furthermore, the current output can be enhanced from 30 to 47 μA and the transferred charges can also be enhanced from 2.6 to 3.9 μC by increasing the amount of water-based GO solution from 5 to 30 μL (Under conditions of 10 N pressure, 0.1 m s^{-1} velocity, 20 mm displacement), but the voltage output decreased slightly (Figure 3g). Figure 3h shows the peak power density and peak current of the GWS-TVNG (N-type Si) under different external loads (Water-based GO solution 8 μL , motion displacement 20 mm, speed 0.1 m s^{-1} , acceleration 2 m s^{-2}). It has a low matched load of 600 Ω , and its maximum peak power density is 5.08 mW m^{-2} . Figure 3i shows the current ($\approx 29 \mu\text{A}$) and voltage ($\approx 0.04 \text{ V}$) output correspond to the maximum peak power density. Compared with the GWS-TVNG (P-type Si) under the

same experimental conditions, the GWS-TVNG (N-type Si) has a lower matched load and also a lower peak power density. It indicates that the silicon wafer type can affect the performance of GWS-TVNG, which has the characteristics of high current output and low impedance.

2.4. Lifetime of GWS-TVNG

TVNG has the output characteristics of high current and low impedance, but the severe wear problem of TVNG will cause rapid attenuation of current density, which is difficult to realize long-term operation with high output. Figure 4a shows stability test of conventional TVNG constituted by copper electrode and P-type Si wafer. The copper electrode slides on the silicon wafer with a sliding distance of 10 mm, sliding velocity of 0.1 m s^{-1} , and sliding acceleration of 2 m s^{-2} . Compared with the initial value of 2.57 μA , the conventional TVNG with P-type Si only retains 21% negative electric output after 3400 times of reciprocating movement. Figure 4a(i,ii) shows the current output before and after 3400 cycles of movement, respectively.

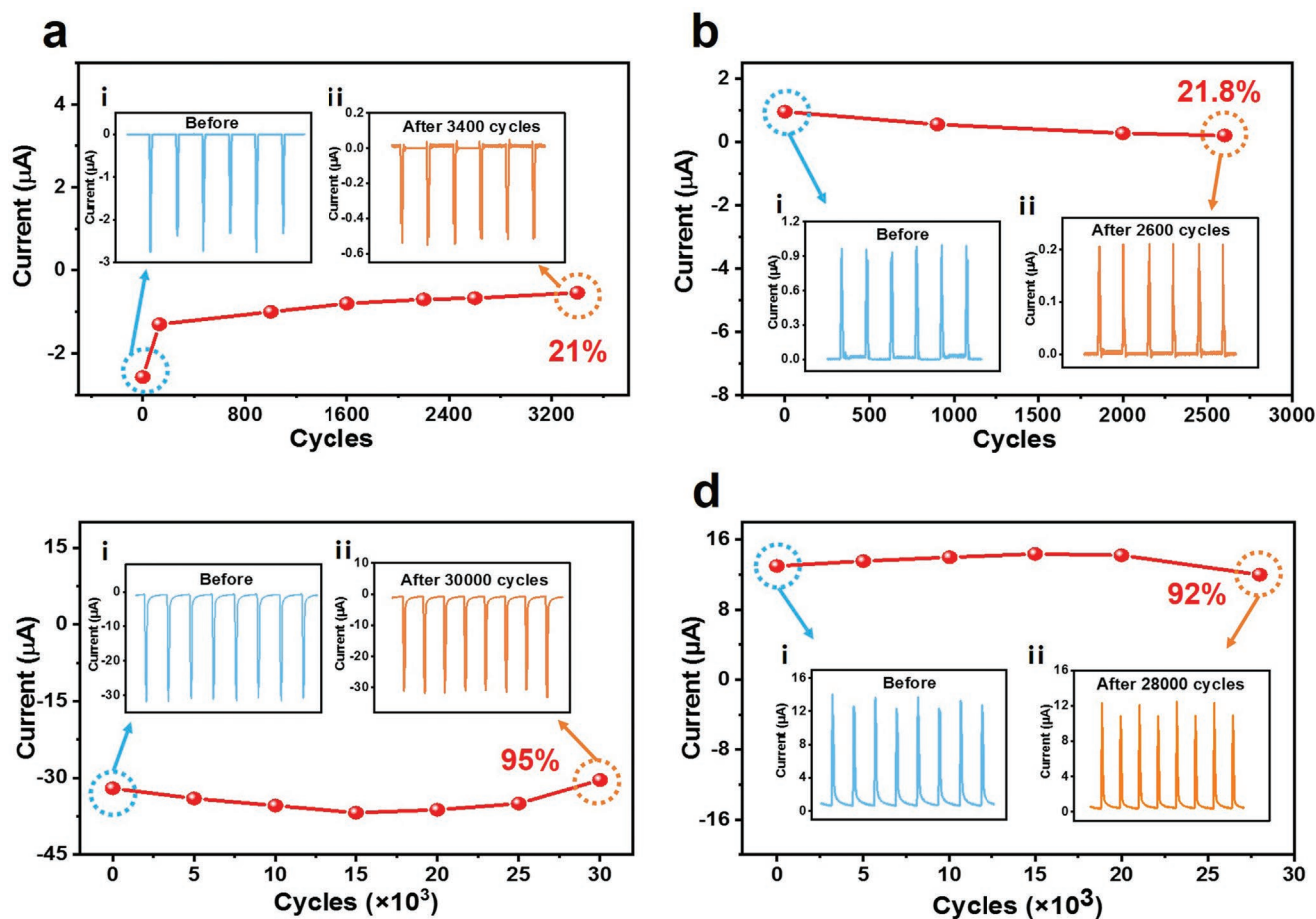


Figure 4. Comparison the lifetime of conventional TVNG (copper block and silicon wafer friction) and GWS-TVNG. a) Stability test. The Cu moves on P-type Si. (motion displacement 10 mm, velocity 0.1 m s^{-1} , acceleration 2 m s^{-2}). b) Stability test. The Cu moves on N-type Si. (motion displacement 10 mm, velocity 0.1 m s^{-1} , acceleration 2 m s^{-2}). c) Stability test. The Cu-G film moves on P-type Si, 2500 μL water-based GO is added to the interface. (motion displacement 10 mm, velocity 0.1 m s^{-1} , acceleration 2 m s^{-2}). d) Stability test. The Cu-G film moves on N-type Si, 2500 μL water-based GO is added to the interface. (motion displacement 10 mm, velocity 0.1 m s^{-1} , acceleration 2 m s^{-2}).

Figure S9a(i,ii) (Supporting Information) shows the scanning electron microscope (SEM) images of copper electrodes before and after the stability test. It can be seen from the SEM images that after 3400 times of reciprocating movement, the copper electrodes appear wear and material transfer, indicating that the hard contact between the copper electrodes and the silicon wafers occur severe wear to cause a sharp drop in output. On the contrary, Figure 4b shows that the lifetime of conventional TVNG was tested by replacing P-type Si with N-type Si. Compared with low initial value of 0.96 μA , after 2600 times of reciprocating movement, the electric output of conventional TVNG with N-type Si only retains 21.8%. Figure 4b(i,ii) shows the current output before and after 2600 cycles of movement, respectively. As shown in Figure S9a,b (Supporting Information), after stability tests, the Si wafers and copper electrode appear significantly scratched. Meanwhile, the abrasion dusts, like the copper particles, are attached to the Si wafers, resulting in the performance degradation of TVNG.

Hence, it is very urgent to find a way to reduce interface wear. When the graphene is used as a lubricant, wear problem will be reduced, this is because the graphene layer prevents direct atoms interlocking between the copper electrode and silicon wafer interface.^[34,35] Thus, we used monolayer graphene films and water-based GO solution materials as an interfacial lubricant to improve the stability and lifetime of GWS-TVNG. Figure S6 (Supporting Information) is a photograph of copper-based monolayer graphene film, a layer of graphene grows on a copper foil of 50 μm , avoiding atomic interlocking at the contact interface. Figure S7 (Supporting Information) is the chemical structure of GO, which not only can provide more carriers to improve current output, but also can be used as an interfacial lubricant to improve lifetime of GWS-TVNG. Figure S8a (Supporting Information) shows the spectral feature of GO at 1594.4 cm^{-1} (G peak) and 1345.3 cm^{-1} (D peak). As shown in Figure S8b,c (Supporting Information), the GO exhibits wrinkled layered structure, which can effectively improve the lubrication effect between friction interface.^[34–36] The copper-based monolayer graphene film was attached to the acrylic substrate, and we designed a tank to hold water-based GO solution to avoid its evaporation. The tank was fixed on P-type Si, and 2500 μL water-based GO solution was injected into the tank to test the stability of GWS-TVNG with P-type Si (Figure 4c). The sliding displacement is 10 mm, the sliding velocity is 0.1 m s^{-1} , and the sliding acceleration is 2 m s^{-2} . After 30 000 times of reciprocating movement, the GWS-TVNG with P-type Si can still retain a high negative electric output of 30.7 μA (retaining 95% compared with initial value of 32.3 μA). To avoid the precipitate of GO, we stir the solution to make it evenly disperse in the water before measuring the output performance of TVNG. In addition, during the sliding process, the water-based GO solution will have molecular motion along with the slider movement, which is also beneficial for the uniform dispersion of GO. As can be seen from Figure 4c, after 30 000 cycles stability tests, the output of GWS-TVNG still retains 95% compared with initial value of 32.3 μA , indicating that the GO still exhibits well lubrication in TVNG after a long working interval. Figure 4c(i,ii) shows the current output before and after 30 000 cycles of movement, respectively. Figure S9c(i,ii) (Supporting Information) shows the SEM images of copper-based

monolayer graphene films before and after the stability test. It can be seen from the SEM images that after 30 000 times of reciprocating movement, the monolayer graphene film folds and falls off, indicating that graphene can reduce wear and improve stability in the process of sliding friction, but cannot guarantee to completely avoid the damage of monolayer graphene film caused by direct contact between Cu–G film and P-type Si. However, compared with copper electrodes, the copper-based monolayer graphene films with lubrication can avoid material transfer of copper particles, as well as the less scratches on the P-type Si (Figure S9c(iii,iv), Supporting Information). Thus, the output stability and lifetime of GWS-TVNG have been significantly improved, accompanied with high current density. In addition, we also tested the output stability and lifetime of GWS-TVNG with N-type Si. The test condition is similar to the GWS-TVNG with P-type Si. After 28 000 times of reciprocating movement (Figure 4d), the GWS-TVNG with N-type Si can still retain output current of 11.96 μA (retaining 92% compared with initial value of 13 μA). The current output before and after the stability test is shown in Figure 4d(i,ii), respectively. As shown in Figure S9d (Supporting Information), the scratches and material transfer could also be reduced.

Compared to conventional TVNG, the current output and lifetime of GWS-TVNG is significantly improved due to the interfacial lubricant of monolayer graphene, water, and GO, where GO is the most important role in the lubrication process (Figure S10 and Note S2, Supporting Information). Specially, water-based GO solution can increase the sliding surface carriers to enhance current density, and reduce the wear between the Cu–G film and the silicon wafer surface due to its excellent lubrication performance. Simultaneously enhancement of current density and lifetime of TVNG can improve its sensitivity for TVNG-based sensor system and lengthen the life-time for TVNG-based energy harvester, which will accelerate the application of TVNG in intelligent factory, the IoT, and distributed sensor direction.

2.5. Applications of the TVNG in Self-Powered Sensing

TVNG can generate high DC output and good durability, which provides a new opportunity for its application in the field of distributed sensing. Based on these features, we combine TVNG with conventional AC-TENG to form a dual-type signals (DS) sensor to meet the needs of distributed sensors for the intelligent factory, big data, and the IoT in future. Based on the device design, the DS sensor can generate AC signal in safe zone and generate DC signal out of safe zone, which is suitable to utilize as vibration sensor to realize threshold monitoring.

Vibration sensor is an important means to monitor the health condition of building structure. Here, a self-powered vibration sensor system is proposed for real-time and continuous detection of vibration characteristics via a DS sensor, which can generate AC or DC signal in different operating zones (Figure 5a). Figure 5a(i) shows the structure of the vibration sensor, the sensor is fixed on the vibration support. Thus, it can generate AC signal in the safe zone, and once outside the safe zone, will produce DC signal and generate signal light alarm (Figure 5a(ii)). Figure 5b is the logical flow chart of the

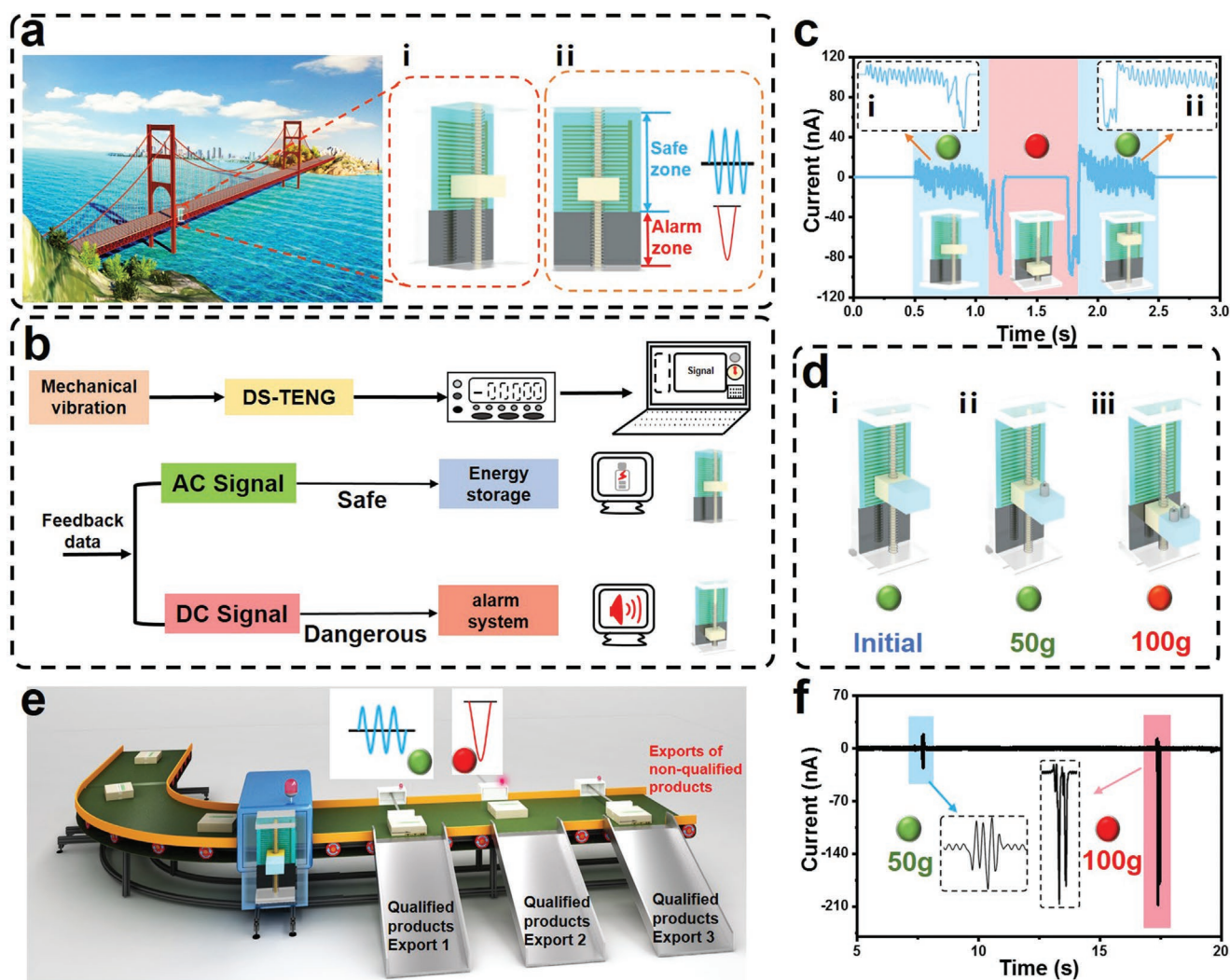


Figure 5. Applications of the DS sensor in self-powered sensing. a) The concept diagram of self-powered DS sensor applied in bridge vibration monitoring. b) The working logic of self-powered vibration monitoring system. c) Signal characteristics of vibration monitoring sensor works in safety zone and beyond safety zone. d) Structure diagram of a self-powered weight monitoring sensor. e) Concept diagram of a self-powered weight monitoring sensor for intelligent factory production line. f) Signal characteristics of weight monitoring sensor works in qualified and non-qualified zones.

vibration monitoring system. The vibration sensor generates the response signal in the corresponding sliding zone, and the signal is collected by the computer through the acquisition card. Figure 5c shows the monitoring signals output of DS sensor, which shows AC signal in the safe zone and DC signal in dangerous zones. Figure 5c(i,ii) are signal characteristics of slider moving from safe zone to dangerous zone and from dangerous zone to safe zone respectively. Meanwhile, according to the peak number of AC pulse signal in the safe zone, the movement displacement can be detected (Figure S11, Supporting Information), accompanied with a maximum response sensitivity of 1 mm (Figure S12, Supporting Information). In addition, DS sensor can monitor the vibration state in real-time and track the vibration trajectory (Movie S1, Supporting Information), which has the characteristics of high sensitivity and multi-signal sensing. It might provide a new application paradigm for TVNG in the field of bridge building structure safety monitoring.

The device can also be used to monitor or classify the weight of goods in the workshop. When the goods are in mass production, the weight of the goods needs within the specified weight. Figure 5d(i) shows the structure of the DS weight monitoring sensor. When the goods are within the specified weight range, the DS weight sensor can generate AC signal and the indicator light is green (Figure 5d(ii)). When the weight of the goods exceeds the specified range, the slider moves to the danger zone, generating a DC signal and the indicator light changes to red (Figure 5d(iii)). Figure S13, (Supporting Information) shows the logic flow of the DS weight sensor real-time monitoring system. Figure 5e is a concept diagram of the DS weight sensor applied to a workshop. Mass productions pass the weight monitoring sensor, qualified products through the push rod sent to the slide for sorting, unqualified products continue through the conveyor belt back to re-processing. Figure 5f shows the sensing signal corresponding to the weight monitoring status in Figure 5d (Dynamic monitoring process in

Movie S2, Supporting Information). When the 50 g weight is placed on the DS weight monitoring sensor, the sensor generates AC signal to indicate the product is qualified. When the 100 g weight is placed on the DS weight monitoring sensor, the sensor generates DC signal to indicate the product is unqualified, and the signal light is red to generate alarm.

The self-powered threshold monitoring sensor system based on DS sensor realizes real-time monitoring information of vibration or realizing good's classification, and track the motion trajectory. The DS sensor can serve as a further potential application for bridge structure safety monitoring and goods weight standard monitoring, accelerating TVNG and TENG sensor applications in IoT, big data, and intelligent factory.

3. Conclusion

In this work, an effective strategy via interface lubrication is proposed to enhance direct-current density and lifetime of TVNG simultaneously. The water-based GO solution is utilized as a lubricant, which can increase the sliding surface carriers to enhance current density, and reduce the wear between the Cu-G film and the silicon wafer surface due to its excellent lubrication performance. For the GWS-TVNG (P-type Si), the peak current output can reach $\approx 155 \mu\text{A}$ (775 mA m^{-2}) and accompanied with ultra-high transfer charges of $6.2 \mu\text{C}$ (31 mC m^{-2}) (under the conditions of $30 \mu\text{L}$ water-based GO solution, 0.1 m s^{-1} velocity and 20 mm displacement). The TVNG via interface lubrication can maintain high current output after 30 000 cycles. In addition, based on its high output, it can combine with AC-TENG to constitute a DS sensor, which can generate AC signal in the safe zone, once outside the safe zone, the DS sensor will produce DC signal and generate a signal light alarm. Thus, DS sensor can be used to monitor bridge vibration and goods' weight monitoring of intelligent factory production line. This work provides an effective strategy to improve the direct-current output and lifetime of TVNG simultaneously and accelerates the future application of TVNG as energy supply unit or self-powered sensor in sensor networks, IoT, and intelligent factories.

4. Experimental Section

Fabrication of the GWS-TVNG: GWS-TVNG consists of a Cu-G film, water-based GO solution, and silicon wafers. The fabrication of the slider: 1) An acrylic with thickness of 5 mm was chosen as the substrate material and laser cutting machine (PLS6.75 universal laser system) was used to cut acrylic of size $10 \text{ mm} \times 10 \text{ mm}$. 2) A $15 \text{ mm} \times 10 \text{ mm}$ Cu-G film (Cu-G film was purchased from Nanjing Muke Nanoscience and Technology Co., LTD., size: $10 \times 10 \text{ cm}^2$, square resistance: $300\text{--}500 \Omega \text{ sq}^{-1}$, monolayer coverage $\geq 96\%$, PMMA+ plasma etching on the back) was cut and glued on the acrylic substrate. Water-based GO solution was purchased from Suzhou Carbon Feng Technology Co., LTD., weight 100 ml , 2 mg mL^{-1} . The silicon wafers of P-type Si ($1\text{--}20 \Omega \text{ cm}$) and N-type Si ($0.001\text{--}0.005 \Omega \text{ cm}$) were purchased from Zhejiang Lijing Photoelectric Technology Co., LTD, with a specification of 4 inches. The crystal was planar oriented along [100], with a diameter of $100 \pm 0.4 \text{ mm}$ and a thickness of $500 \pm 10 \mu\text{m}$. The back electrode was coated with Au film ($\approx 2 \mu\text{m}$) on the matte surface of the silicon wafer by magnetron

sputtering (35 min). Finally, copper wire was used to connect the Cu-G electrode and the back electrode. GWS-TVNG was formed by adding water-based GO solution between the Cu-G film and the silicon wafer.

Fabrication of Water-Based GO Solution Tank: 1) An acrylic of thickness 5 mm was chosen as the substrate, and laser cutting machine (PLS6.75 general laser system) was used to cut the size of two $10 \text{ mm} \times 20 \text{ mm}$, two $10 \text{ mm} \times 40 \text{ mm}$, and a $30 \text{ mm} \times 40 \text{ mm}$ as acrylic substrate. 2) Acrylic glue was used to stick five acrylic substrates into a tank.

Fabrication of the DS Sensor: DS includes AC-TENG and TVNG. The fabrication of AC-TENG: 1) Acrylic with thickness of 5 mm was selected as the substrate, and laser cutting machine (PLS6.75 universal laser system) was used to cut the size of $60 \text{ mm} \times 30 \text{ mm}$ acrylic substrate. 2) The sponge with thickness of 2 mm was chosen as the buffer layer, and a $30 \text{ mm} \times 40 \text{ mm}$ sponge was cut. The sponge was glued along the edge of the acrylic substrate ($60 \text{ mm} \times 30 \text{ mm}$). 3) The grid electrodes with different precision (1 mm, 1.5 mm) sizes were drawn by AutoCAD2018 drawing software. 4) To make flexible printed circuit board (PCB), the size of $30 \text{ mm} \times 40 \text{ mm}$ grid copper electrode (thickness of $35 \mu\text{m}$) was glued on the acrylic substrate as the induction electrode. 5) The copper electrode was coated with a FEP film with a thickness of $150 \mu\text{m}$ as the friction layer. The fabrication of TVNG: 1) Thick kapton double-sided tape (1.6 mm) was glued to the remaining $20 \text{ mm} \times 30 \text{ mm}$ position below the $60 \text{ mm} \times 30 \text{ mm}$ acrylic substrate. 2) P-type Si ($1\text{--}20 \Omega \text{ cm}$) of size $20 \text{ mm} \times 30 \text{ mm}$ was cut with a glass knife. The silicon wafer was glued onto the Kapton tape so that the silicon height is consistent with the friction layer height. AC-TENG and TVNG used the same slider. The fabrication of the slider: 1) An acrylic with a thickness of 3 mm was chosen as the substrate, and $25 \text{ mm} \times 2 \text{ mm}$ acrylic was cut with a laser cutting machine (PLS6.75 universal laser system). 2) A 2 mm sponge of the same size was glued to the acrylic substrate material. 3) The slider electrode of size $1 \text{ mm} \times 25 \text{ mm}$ was glued on the sponge.

Measurement: Including GWS-TVNG performance test and self-powered dual-type signals sensor test. The sliding process was conducted by a linear motor (TSMV120-1S). The short-circuit current, open-circuit voltage, and transferred charges of the GWS-TVNG and AC-TENG was measured by a programmable electrometer (Keithley model 6514).

Supporting Information

Supporting Information is available from the Wiley Online Library or from the author.

Acknowledgements

W.Q., Z.Z., and L.Z. contributed equally to this work. Research was supported by the National Key R & D Project from Minister of Science and Technology (2021YFA1201602), National Natural Science Foundation of China (Grant no. 61774016, 22109013), Fundamental Research Funds for the Central Universities (E1E46802), and China Postdoctoral Science Foundation (2021M703172, 2021M703171).

Conflict of Interest

The authors declare no conflict of interest.

Data Availability Statement

The data that support the findings of this study are available from the corresponding author upon reasonable request.

Keywords

high direct-current, interface lubrication, self-powered sensors, tribovoltaic nanogenerators

Received: July 25, 2022
Revised: August 23, 2022
Published online:

- [1] Z. L. Wang, W. Wu, *Angew. Chem., Int. Ed.* **2012**, *51*, 2.
[2] Z. L. Wang, *Mater. Today* **2017**, *20*, 74.
[3] F. Fan, Z. Tian, Z. L. Wang, *Nano Energy* **2012**, *1*, 328.
[4] X. Yin, D. Liu, L. Zhou, X. Li, G. Xu, L. Liu, S. Li, C. Zhang, J. Wang, Z. L. Wang, *Adv. Funct. Mater.* **2020**, *30*, 2002547.
[5] S. Li, Z. Zhao, D. Liu, J. An, Y. Gao, L. Zhou, Y. Li, S. Cui, J. Wang, Z. L. Wang, *Adv. Mater.* **2022**, *10*, 1002.
[6] S. Li, L. Liu, Z. Zhao, L. Zhou, X. Yin, X. Li, Y. Gao, C. Zhang, Q. Zhang, J. Wang, Z. L. Wang, *ACS Nano* **2020**, *14*, 2475.
[7] M. Xu, P. Wang, Y. Wang, S. Zhang, A. Wang, C. Zhang, Z. Wang, X. Pan, Z. L. Wang, *Adv. Energy Mater.* **2018**, *8*, 1702432.
[8] X. Xiao, X. Zhang, S. Wang, H. Ouyang, P. Chen, L. Song, H. Yuan, Y. Ji, P. Wang, Z. Li, M. Xu, Z. L. Wang, *Adv. Energy Mater.* **2019**, *9*, 1902460.
[9] X. Hang, X. Xiang, J. Nie, D. Peng, F. Yang, Z. Wu, H. Jiang, Z. Xu, Q. Zheng, *Nat. Commun.* **2021**, *12*, 2268.
[10] Z. L. Wang, A. C. Wang, *Mater. Today* **2019**, *30*, 34.
[11] Z. Zhang, D. Jiang, J. Zhao, G. Liu, T. Bu, C. Zhang, Z. L. Wang, *Adv. Energy Mater.* **2020**, *10*, 1903713.
[12] R. Xu, Q. Zhang, J. Wang, D. Liu, J. Wang, Z. L. Wang, *Nano Energy* **2019**, *66*, 104185.
[13] X. Xu, J. Li, X. Tao, Q. Yan, H. Wu, Z. Guan, L. Liu, X. Chen, W. Ou-Yang, *Nano Energy* **2022**, *94*, 106957.
[14] G. Liu, J. Liu, W. Dou, *Nano Energy* **2022**, *96*, 107034.
[15] M. Benner, R. Yang, L. Lin, M. Liu, H. Li, J. Liu, *ACS Appl. Mater. Interfaces* **2022**, *14*, 2968.
[16] Y. Chen, Z. Zhang, Z. Wang, T. Bu, S. Dong, W. Wei, Z. Chen, Y. Lin, Y. Lv, H. Zhou, W. Sun, C. Zhang, *ACS Appl. Mater. Interfaces* **2022**, *14*, 24020.
[17] J. Meng, Z. Guo, C. Pan, L. Wang, C. Chang, L. Li, X. Pu, Z. Wang, *ACS Energy Lett.* **2021**, *6*, 2442.
[18] M. Zheng, S. Lin, L. Xu, L. Zhu, Z. L. Wang, *Adv. Mater.* **2020**, *32*, 2000928.
[19] H. Yuan, Z. Xiao, J. Wan, Y. Xiang, G. Dai, H. Li, J. Yang, *Adv. Energy Mater.* **2022**, *12*, 2200550.
[20] Z. Zhang, Z. Wang, Y. Chen, Y. Feng, S. Dong, H. Zhou, Z. L. Wang, C. Zhang, *Adv. Mater.* **2022**, *34*, 2200146.
[21] Z. Wang, Z. Zhang, Y. Chen, L. Gong, S. Dong, H. Zhou, Y. Lin, Y. Lv, G. Liu, C. Zhang, *Energy Environ. Sci.* **2022**, *15*, 2366.
[22] L. Ren, A. Yu, W. Wang, D. Guo, M. Jia, P. Guo, Y. Zhang, Z. L. Wang, J. Zhai, *Nano Lett.* **2021**, *21*, 10099.
[23] J. Meng, Z. Guo, C. Pan, L. Wang, C. Chang, L. Li, X. Pu, Z. L. W, *ACS Energy Lett.* **2021**, *6*, 2442.
[24] S. Lin, Y. Lu, S. Feng, Z. Hao, Y. Yan, *Adv. Mater.* **2019**, *31*, 1804398.
[25] M. Zheng, S. Lin, Z. Tang, Y. Feng, Z. L. Wang, *Nano Energy* **2021**, *83*, 105810.
[26] M. Zheng, S. Lin, L. Zhu, Z. Tang, Z. L. Wang, *Adv. Mater. Interfaces* **2021**, *9*, 2101757.
[27] S. Lin, X. Chen, Z. L. Wang, *Nano Energy* **2020**, *76*, 105070.
[28] J. Bian, L. Nicola, *Tribol. Int.* **2021**, *156*, 106837.
[29] A. Šutka, M. Zubkins, A. Linarts, L. Lapčinskis, K. Mālnieks, O. Verners, A. Sarakovskis, R. Grzibovskis, J. Gabrusenoks, E. Strods, K. Smits, V. Vibornijs, L. Bikse, J. Purans, *J. Phys. Chem. C* **2021**, *125*, 14212.
[30] X. Luo, L. Liu, Y. Wang, J. Li, A. Berbille, L. Zhu, Z. L. Wang, *Adv. Funct. Mater.* **2022**, *32*, 2113149.
[31] L. Zhang, H. Cai, L. Xu, L. Ji, D. Wang, Y. Zheng, Y. Feng, X. Sui, Y. Guo, W. Guo, F. Zhou, W. Liu, Z. L. Wang, *Matter* **2022**, *5*, 1.
[32] D. Yang, L. Zhang, N. Luo, Y. Liu, W. Sun, J. Peng, M. Feng, Y. Feng, H. Wang, D. Wang, *Nano Energy* **2022**, *99*, 107370.
[33] Z. Zhang, T. He, J. Zhao, G. Liu, Z. L. Wang, C. Zhang, *Mater. Today Phys.* **2021**, *16*, 100295.
[34] Y. Liu, X. Ge, J. Li, *Appl. Mater. Today* **2020**, *20*, 100662.
[35] H. Kinoshita, Y. Nishina, A. Alias, M. Fujii, *Carbon* **2014**, *66*, 720.
[36] J. Bian, L. Nicola, *Tribol. Int.* **2021**, *156*, 106837.